Anal. Bioanal. Electrochem., Vol. 9, No. 5, 2017, 640-659

Analytical & Bioanalytical Electrochemistry

2017 by CEE
www.abechem.com

Full Paper

Adsorption and Corrosion Inhibition of Mild Steel by ((Z)-4-((2,4-dihydroxybenzylidene)amino)-5-methy-2,4 dihydro-3H-1,2,4-triazole-3-thione) in 1M HCl :Experimental and Computational Study

Imane Merimi,[1] Yasser El Ouadi,[2] Kashif Rahmani Ansari,[3] Hassan Oudda,[1] Belkheir Hammouti,[2] Mumtaz Ahmad Quraishi,[3,*] Fawzia Faleh Al-blewi,[4] Nadjet Rezki,[4,5] Mohamed Reda Aouad[4,5] and Mousslim Messali[4]

[1]*Laboratory of Separation Processes, Université Ibn Tofail, Faculté des Sciences, Kenitra, Morocco*

[2]*Laboratoire de chimie analytique appliquée, matériaux et environnement (LC2AME), Faculté des Sciences, B.P. 717, 60000 Oujda, Morocco*

[3]*Department of Chemistry, Indian Institute of Technology (Banaras Hindu University), Varanasi-221005 (U.P.) - INDIA*

[4]*Department of Chemistry, Taibah University, 30002, Al-Madina Al-Mounawara, Saudi Arabia*

[5]*Laboratoire de Chimie & Electrochimie des Complexes Métalliques (LCECM) USTO-MB, University of Sciences and Technology Mohamed Boudiaf, BP 1505 Oran, El M`nouar, Algeria*

*Corresponding Author, Tel.: +91-9307025126; Fax: +91- 542- 2368428

E-Mail: maquraishi.apc@itbhu.ac.in

Received: 17 April 2017 / Received in revised form: 22 May 2017 / Accepted: 18 June 2017 / Published online: 15 August 2017

Abstract- The present study aims at investigating the corrosion inhibition performance of a new triazole inhibitor namely (Z)-4-((2,4-dihydroxybenzylidene) amino)-5-methy-2,4-dihydro-3H-1,2,4-triazole-3-thione on mild steel corrosion in 1.0 M HCl solution using weight loss, electrochemical impedance spectroscopy, potentiodynamic polarization

www.SID.ir

measurements and density functional (DFT) methods. The results show that inhibition efficiency increases with increase in the inhibitor concentration and maximum inhibition efficiency of 80.74% was obtained at a concentration of 10^{-3} M. The corrosion behavior was also studied in the absence and presence of inhibitor at various concentrations in the temperature range of 318-348 K. Potentiodynamic polarization results showed that the inhibitor is mixed-type. The Nyquist plots showed that on increasing the inhibitor concentration charge-transfer resistance increased and double-layer capacitance values decreased thereby suggesting that corrosion inhibition is charge transfer controlled process and inhibition occurs due to the adsorption of inhibitor molecules on the metal surface. The adsorption of inhibitors followed Langmuir a isotherm Quantum chemical calculations very well supported the experimental results.

Keywords- Mild steel, Corrosion inhibition, Adsorption, Potentiodynamic polarization, Electrochemical impedance, Quantum chemical calculation

1. INTRODUCTION

The study of the corrosion inhibition of metals in acid solutions is an important industrial topic. Acidic solutions especially hydrochloric acid solutions (HCl), are widely used in various industrial processes, such as oil well acidification, acid pickling, acid cleaning, and acid descaling, which generally leads to serious metallic corrosion [1].

The use of inhibitors is one of the most practical methods for protection against corrosion and prevention of unexpected metal dissolution and acid consumption, especially in acidic medium.

Heterocyclic compounds constitute a potential class of corrosion inhibitors. Compounds containing both nitrogen and sulphur atoms in the same molecule are of particular importance as they provide better inhibition efficiency as compared to compounds containing nitrogen and sulphur alone [2-6].

In continuation of work on hetrocyclic compounds [7], we have investigated the effect of new triazole namely (Z)-4-((2,4-dihydroxybenzylidene)amino)-5-methy-2,4-dihydro-3H-1,2,4-triazole-3-thione on the corrosion inhibition of mild steel in 1 M HCl medium by electrochemical impedance spectroscopy (EIS) and potendiodynamic polarization methods. The selection of this compound as corrosion inhibitor is based on the fact that it is non toxic and contains three nitrogen atoms, sulphur and two hydroxyl groups in the same molecule which act as the absorption centers through which this inhibitor can get adsorbed on the mild steel surface and reduces the corrosion rate of mild steel [8]. In addition, quantum chemical calculations were calculated using DFT method to support the experimental results. Figure 1 shows the molecular structure of the triazole derivative.

Archive of SID

www.SID.ir

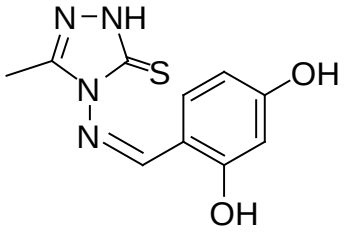

Fig. 1. Chemical structure of the inhibitor

2. EXPERIMENTAL

2.1. Materials

The test material in this study is mild steel with the chemical composition (in wt%) of 0.09%P, 0.01% Al, 0.38% Si, 0.05% Mn, 0.21% C, 0.05% S and the remainder iron (Fe). The steel samples were pre-treated prior to the experiments by grinding with emery paper SiC (220, 400, 800, 1000 and 1200); rinsed with distilled water, degreased in acetone, washed again with bidistilled water and then dried at room temperature before use.

2.2. Solutions

The aggressive solutions of 1.0 M HCl were prepared by the dilution of analytical grade 37% HCl with distilled water. The concentration range of (Z)-4-((2,4-dihydroxybenzylidene)amino)-5-methy-2,4-dihydro-3H-1,2,4-triazole-3-thione used was 10^{-6} M to 10^{-3} M.

2.3. Weight loss study

Weight loss experiments were performed according to the standard methods [9]. The mild steel sheets of 1×1×0.1cm dimension were immersed in a 250 mL beaker containing 100 mL of 1.0 M HCl solution with and without addition of different concentrations of inhibitor. All the aggressive acid solutions were open to air. After 6 hours of immersion, the specimens were taken out, washed, dried, and weighed accurately. In order to get good reproducibility, all measurements were performed three times and average values were reported. The inhibition efficiency (η_{WL}%) and surface coverage (θ) were calculated as follows:

$$C_R = \frac{W_b - W_a}{At} \quad (1)$$

$$\eta_{WL}(\%) = \left(1 - \frac{w_i}{w_0}\right) \times 100 \quad (2)$$

$$\theta = 1 - \frac{w_i}{w_0} \quad (3)$$

Archive of SID

www.SID.ir

Where W_b and W_a are the specimen weight before and after immersion in the tested solution, w_0 and w_i are the values of weight losses of mild steel in uninhibited and inhibited solutions, respectively, A the total area of the mild steel specimen (cm^2) and t is the exposure time (h).

2.4. Electrochemical measurements

The electrochemical measurements were carried out using Volta lab (Tacussel-Radiometer PGZ 100) potentiostat and controlled by Tacussel corrosion analysis software model (Voltamaster 4) at under static condition. The corrosion cell used had three electrodes. The reference electrode was a saturated calomel electrode (SCE). A platinum electrode was used as auxiliary electrode (surface area of 1 cm^2). The working electrode was mild steel with the surface area of 0.32 cm^2. The working electrode was immersed in test solution for 30 min in order to get the steady state open circuit potential (E_{ocp}). After measuring the E_{ocp}, the electrochemical measurements were performed. All electrochemical tests have been performed in aerated solutions at 308 K. The EIS experiments were conducted in the frequency range of 100 kHz to 0.1 Hz at open circuit potential, with an amplitude of 10 mV per decade peak-to-peak. The semicircle can be best fitted through the data points in the Nyquist plot using a non-linear least square fit so as to give the intersections with the *x*-axis. The inhibition efficiency of the inhibitor was calculated from the charge transfer resistance values using the following equation:

$$\eta_z\% = \frac{R_{ct}^{i} - R_{ct}^{\circ}}{R_{ct}^{i}} \times 100 \quad (4)$$

Where, R°_{ct} and R^{i}_{ct} are the charge transfer resistance in absence and in presence of inhibitor, respectively.

The potentiodynamic polarization measurements of mild steel substrate in inhibited and uninhibited solution were scanned from cathodic to the anodic direction in the potential range of ±250 mV, with a scan rate of 1 mV s^{-1}. The linear Tafel segments of anodic and cathodic curves were extrapolated to corrosion potential to obtain corrosion current densities (I_{corr}). From the polarization curves obtained, the corrosion current (I_{corr}) was calculated by curve fitting using the equation:

$$I = I_{corr}\left[exp\left(\frac{2.3\Delta E}{\beta_a}\right) - exp\left(\frac{2.3\Delta E}{\beta_c}\right)\right] \quad (5)$$

The inhibition efficiency was evaluated from the measured I_{corr} values using the following relationship:

Archive of SID

www.SID.ir

$$\eta_{\text{Tafel}}(\%) = \frac{I_{\text{corr}} - I_{\text{corr(i)}}}{I_{\text{corr}}} \times 100 \quad (6)$$

Where I_{corr} and $I_{\text{corr(i)}}$ are the corrosion current densities for steel electrode in the uninhibited and inhibited solutions, respectively.

2.5. Quantum chemical calculations

Complete geometry optimization of the inhibitor molecules were performed using density functional theory (DFT) with Beck's three-parameter exchange functional along with Leee Yange Parr non-local correlation functional (B3LYP) with 6-31G basis set using the Gaussian 03 program package [10]. It is well known that the corrosion process undergoes in the aqueous phase, so it is computationally suitable to include the effect of solvent. Frontier molecular orbitals (HOMO and LUMO) were used to interpret the adsorption of inhibitor molecules on the metal surface. According to DFT-Koopman's theorem [11,12], the ionization potential (I) is approximated as the negative of the highest occupied molecular orbital energy (E_{HOMO}) and the negative of the lowest unoccupied molecular orbital energy (E_{LUMO}) is related to the electron affinity (A).

$$I = -E_{HOMO} \quad (7)$$

$$A = -E_{LUMO} \quad (8)$$

Natural bond orbital (NBO) analysis [13] was performed to evaluate the electron density distributions. The electron density plays an important role in calculating the chemical reactivity parameters. The global reactivates include electronegativity (χ), global hardness (η) and the global softness (σ). They can be calculated from the following equations:

$$\chi = \frac{I + A}{2} \quad (9)$$

$$\eta = \frac{I - A}{2} \quad (10)$$

$$\sigma = \frac{1}{\eta} = -\frac{2}{E_{HOMO} - E_{LUMO}} \quad (11)$$

The local reactivity has been analyzed by means of Fukui indices [14], an indication of the reactive centers within the molecules. These measurements provide the chemical reactivity, as well as an indicative of the reactive regions, nucleophilic and electrophilic behavior of the molecule [15]. The condensed Fukui functions were found by taking the finite difference approximations from Mulliken population analysis of atoms in inhibitor molecules, depending on the direction of the electron transfer.

$$f_k^+ = q_k(N+1) - q_k(N) \quad (12)$$

Archive of SID

www.SID.ir

$$f_k^- = q_k(N) - q_k(N-1) \quad (13)$$

Where q (N), q (N+1), and q (N-1) are the electronic population of the atom k in neutral, cationic and anionic systems respectively [16].

3. RESULTS AND DISCUSSION

3.1. Open circuit potential

Before the electrochemical measurements, the variation in Eocp for every second up to 30 min was measured for mild steel immersed in 1MHCl with and without inhibitor. Associated Eocp *vs*. time curves in absence and in the presence of optimum concentration of inhibitor are presented in Fig. 2.

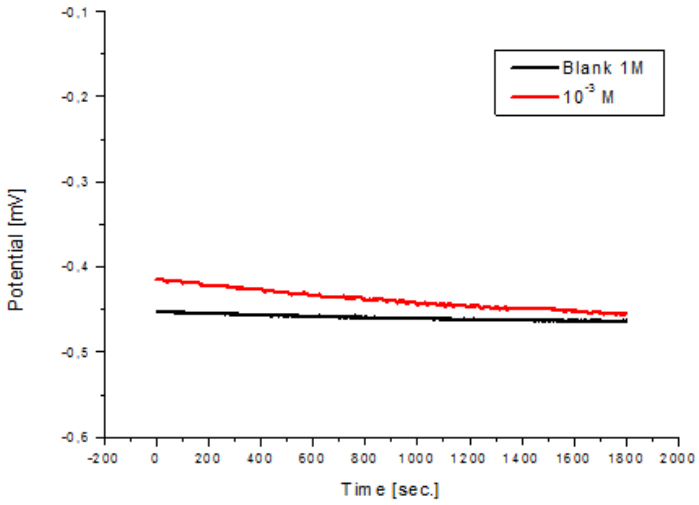

Fig. 2. OCP *vs*. time measurements in absence and presence of optimum concentration of inhibitor

In absence of inhibitor molecules, the curve starts nearly at -450 mV and display stable plateau throughout the observed period of study. On the other hand, in presence of inhibitor the Eocp *vs*. time curve was observed to be more positive compared in absence of inhibitor and decreases until 1650 s after which it builds up a constant potential until the 1800th second.

3.2. Potentiodynamic polarization curves

The potentiodynamic measurement results of mild steel in 1.0 M HCl solution without and with different inhibitor concentrations are shown in Fig. 3. The polarization parameters namely corrosion current density (i_{corr}), corrosion potential (E_{corr}), anodic Tafel slope (β_a),

www.SID.ir

cathodic Tafel slope (β_c) and percentage inhibition efficiency (η_T%) were calculated from the Tafel curves and are given in Table 1. It can be observed from Fig. 2, both the cathodic and anodic reactions were suppressed with the addition of inhibitor, which suggested that inhibitor reduced both the anodic dissolution as well as retardation of hydrogen gas evolution reactions respectively [17].

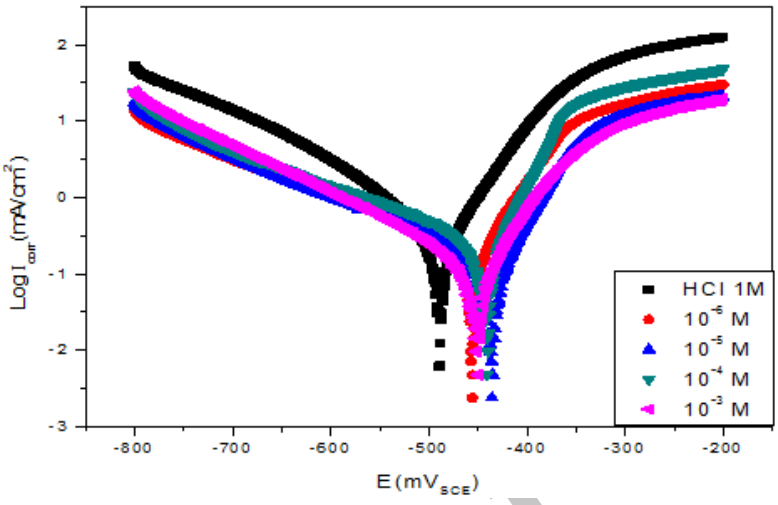

Fig. 3. Polarization curves for mild steel in 1.0 M HCl in the absence and presence of different concentration of inhibitor

It is clear from Table 1 that after increasing the concentration of inhibitor, the inhibition efficiency increased, while the corrosion current density decreased due to adsorption of inhibitor on the mild steel surface. The minor shift in E_{corr} value (60 mV) towards positive direction in the presence of inhibitor as compared to the E_{corr} value in the absence of inhibitor indicate the mixed mode of inhibitor action with predominant control by anodic reaction [18, 19].

Table 1. The electrochemical parameters for mild steel in 1.0 M HCl solution without and with different concentration of inhibitor at 308 K

Inhibitor concentrations	**$-E_{corr}$ (mV_{SCE})**	**β_a (mV/dec)**	**$-\beta_c$ (mV/dec)**	**i_{corr} (mA/cm^2)**	**η_T (%)**
HCl 1M	490	77	155	0.655	-
10^{-6} M	456	57	128	0.1691	70.12
10^{-5} M	437	55	195	0.1435	78.09
10^{-4} M	441.	42	166	0.14	78.61
10^{-3} M	451.	63	154	0.122	81.37

Archive of SID

www.SID.ir

3.3. Electrochemical impedance spectroscopy studies

The Nyquist plots obtained from the EIS measurements for mild steel in 1.0 M HCl solutions at 308 K are shown in Fig. 4. The plots are characterized by a depressed semicircle reflects that corrosion process was mainly controlled by charge transfer mechanism and surface in-homogeneity of structural or interfacial origin, such as those found in adsorption processes respectively [20]. The diameter of semicircle in presence of inhibitor increased with increase in inhibitor concentration, which represents that mild steel surface becomes more resistance towards corrosion due to adsorption of inhibitor molecules. The charge transfer resistance values (R_{ct}) were calculated from the difference between impedance values at lower and higher frequencies as suggested by Haruyama et al. [21]. The double layer capacitance (C_{dl}) was obtained from the following equation [22]:

$$f\left(-Z_{img}\right)=\frac{1}{2\pi C_{dl}R_{ct}} \qquad (14)$$

Where Z_{img} is the frequency of maximum imaginary components of the impedance and R_{ct} is the charge transfer resistances.

The calculated electrochemical parameters of EIS measurements are listed in Table 2.

Table 2. EIS parameters for the corrosion of mild steel in 1.0 M HCl containing inhibitor at 308 K

Inhibitor concentration	R_{ct} **(Ω.cm^2)**	f_{max} **(Hz)**	C_{dl} **(μF/cm^2)**	η_z **(%)**
HCl 1M	16.27	100	97.82	-
10^{-6} M	50.48	50	63.06	67.77
10^{-5} M	70.39	50	45.22	76.88
10^{-4} M	81.41	50	39.1	80.01
10^{-3} M	88.8	50	35.84	81.67

From the Table, it is clear that as the inhibitor concentration increased, the R_{ct} values increased and the C_{dl} values decreased, which is due to a decrease in local dielectric constant and/or an increase in the thickness of the electrical double layer, suggesting that the inhibitor molecules acted by adsorption at the metal/solution interface [23]. In addition, the inhibitor molecules may reduce the capacitance by increasing the double layer thickness according to the Helmholtz model [24]:

$$\delta_{org}=\frac{\varepsilon_0\varepsilon A}{C_{dl}} \qquad (15)$$

Archive of SID

www.SID.ir

Where ε is the dielectric constant of the medium, ε_0 is the dielectric constant in vacuum,

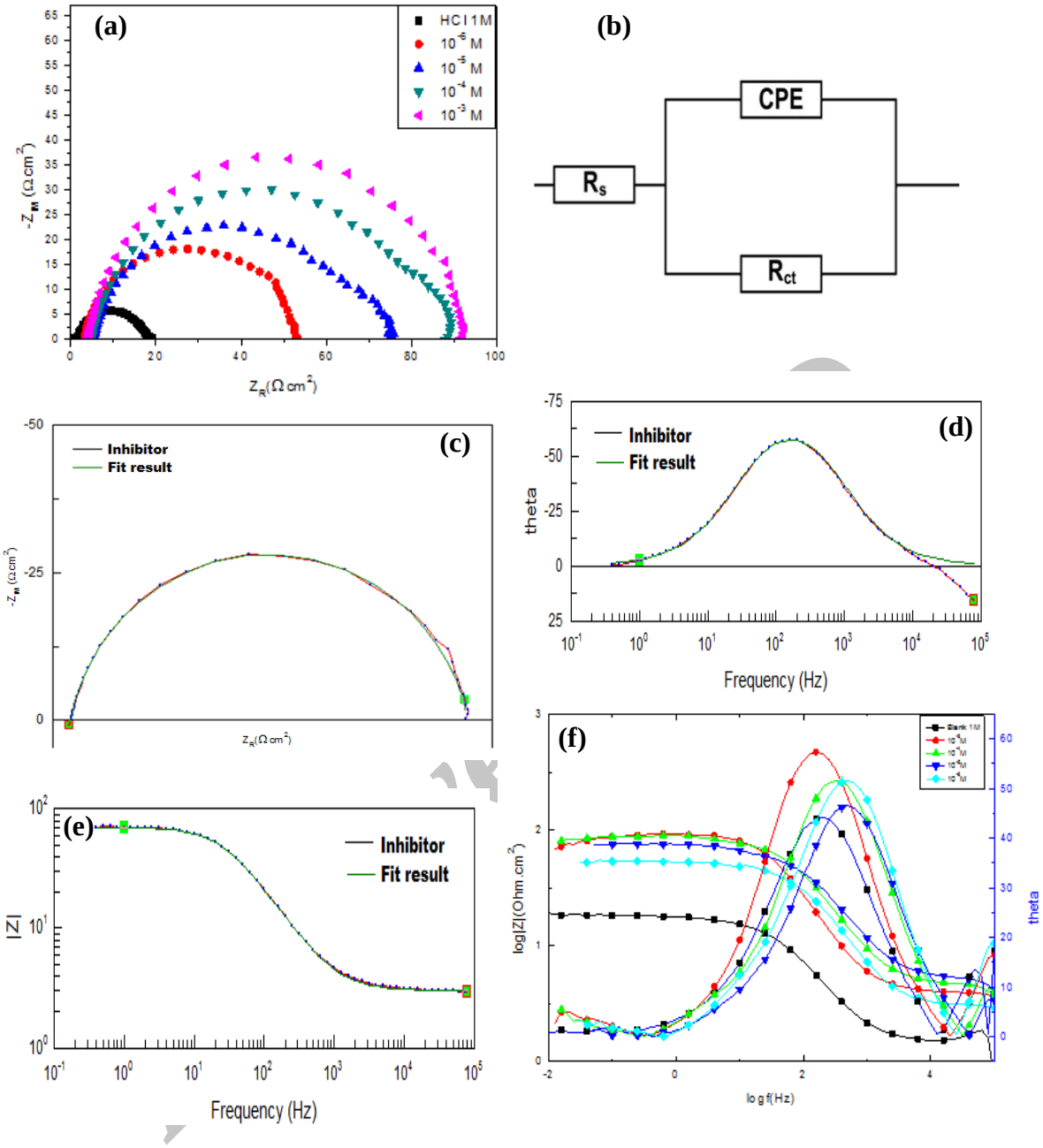

Fig. 4. (a) Nyquist plots recorded for mild steel in 1.0 M HCl solutions without and with differents concentrations of inhibitor; **(b)** Equivalent circuit used to simulate the EIS diagram; **(c)** Fitted Nyquist plot and Bode plot for PZ-1; **(d)** Fitted phase angle plot; **(e)** Fitted Bode plot; **(f)** Bode (log f *vs*. log|Z|) and phase angle (log f *vs*. theta) plots of impedance spectra for mild steel in 1 M HCl in absence and presence of different concentration of inhibitor

A is the electrode surface area and δ_{org} is the thickness of the protective layer. The impedance diagram can be modeled by the addition of solution resistance (R_s), constant phase element (CPE) and charge transfer resistance (R_{ct}) and are shown in Fig. 4b.[25]. The

www.SID.ir

equivalent electrical circuits used provide a good fit over the impedance experimental data and are shown in Fig. 4c-e [26-29].

The Bode and phase angle plots for mild steel in 1 M HCl in absence and presence of different optimum concentration of inhibitor is shown in Fig. 4f. The Bode phase angle plots have only one maximum i.e. one time constant at the intermediate frequencies and broadening of this maximum in presence of inhibitor suggests the formation of a protective layer on mild steel surface. Also increase in the phase angle values in presence of inhibitor reveals their inhibitive action. The impedance values in presence of inhibitor are larger than their absence (Fig. 4f), which indicates the reduction of corrosion process.

3.4. Weight loss study

3.4.1. Effect of inhibitor concentration

Table 3 shows the results obtained from weight loss measurements for mild steel in 1.0 M HCl solutions in the absence and presence of different concentrations of inhibitor. It has been observed from the results that the η_{WL}% of inhibitor increases from 64.84% to 80.47% with the increase in inhibitor concentration from 10^{-6} to 10^{-3} M. Indeed, corrosion rate values of mild steel decreases from 0.1125 to 0.0625 mg/cm^2/ h on the addition of inhibitor. The increase in efficiency may be due to the blocking effect of the surface by both adsorption and film formation mechanisms, which decrease the effective area of corrosion attack [30]. The inhibiting performance exhibited by the compound may be due to the planar aromatic rings and presence of N, S atoms and π electrons [31].

Table 3. Weight loss values of various concentrations of (inhibitor) in 1.0 M HCl solution

Concentrations	**C_R(mg/cm^2 x h)**	**θ**	**η_{WL} %**
HCl (1M)	0.32	-	-
10^{-6} M	0.1125	0.64	64.84
10^{-5} M	0.0801	0.74	74.96
10^{-4} M	0.0726	0.77	77.31
10^{-3} M	0.0625	0.8	80.47

3.4.2. Adsorption isotherm

The extent of adsorption of an inhibitor on the metal surface is usually influenced by the parameters such as the nature, chemical structure, distribution of charge on the molecule and charge on the metal. Basic information regarding the nature of interaction of the adsorbed

Archive of SID

www.SID.ir

inhibitor molecule and the mild steel surface can be elucidated using adsorption isotherm. The surface coverage θcan be obtained by using the well-known formula η=WL%/100. The value of θ increased with increase in inhibitor concentration, demonstrating the more pronounced adsorption of inhibitor on the metal surface. The θ value was fitted to various isotherms like Langmuir, Freundlich, Temkin and Frumkin. Langmuir was found to give the best description on the adsorption of inhibitor. The equation corresponding to Langmuir adsorption isotherm is:

$$\frac{C_{inh}}{\theta} = \frac{1}{K_{ads}} + C_{inh} \qquad (16)$$

Where C_{inh} represents the concentration of the inhibitor in mol/L and K denotes the adsorption-desorption equilibrium constant. A plot of C_{inh} *vs* C_{inh}/θ gave a straight line with a slope around unity (Fig. 5). This suggests monolayer adsorption of inhibitor on the surface of mild steel. The values of thermodynamic parameters such as K_{ads} , ΔG°_{ads}, R^2 and the correlation coefficient R^2 were enumerated in Table 4.

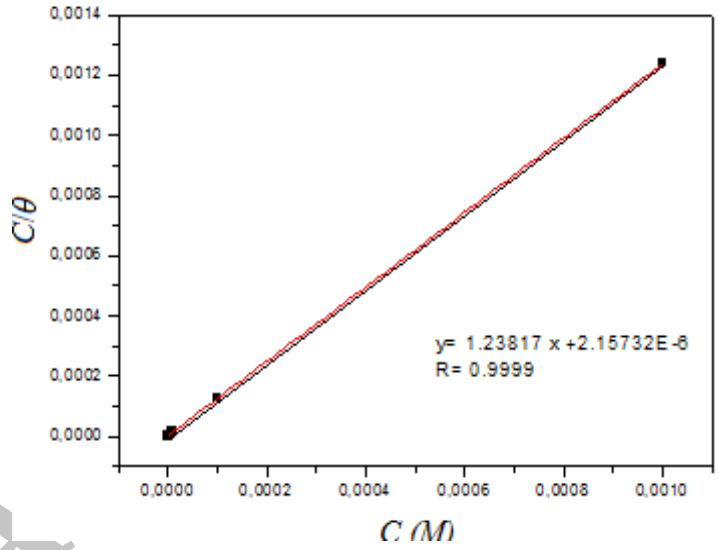

Fig. 5. The Langmuir adsorption isotherm plots for the adsorption of inhibitor in 1.0 M HCl on the surface of mild steel

Table 4. Thermodynamic parameters for mild steel in 1.0 M HCl in the presence of inhibitor at 308 K

Measurements	K_{ads} **L mol^{-1}**	ΔG°_{ads} **kJ mol-1**	**(R^2)**
Weight loss	4.63×10^5	-43.69	0.9999

www.SID.ir

$\Delta G°_{ads}$calculated from the slope of Langmuir adsorption isotherm using the following equation:

$$\Delta G^{\circ}_{ads} = -RTLn(55.5K_{ads}) \quad (17)$$

Where R is gas constant and T is absolute temperature of experiment and the constant value of 55.5 is the concentration of water in solution in mol L^{-1}. In Fig. 5, the intercept on the vertical axis is the value of 1/ K_{ads}.

Generally, values of ΔG_{ads} up to -20 kJ/mol, the types of adsorption were regarded as physisorption, the inhibition acts due to the electrostatic interactions between the charged molecules and the charged metal, while values around -40 kJ/mol or smaller are associated with chemisorption as a result of sharing or transfer of electrons from organic molecules to the metal surface to form a coordinate type of bond (chemisorption) [32].

Then according to Eq. (17), we calculated the ΔG_{ads}=-43.69 kJ/mol. Therefore it can be concluded that the adsorption of the inhibitor on the mild steel surface is mainly the chemical adsorption inevitably accompanied by the physical adsorption.

3.4.3. Influence of Temperature

The study of the influence of temperature on the rate of corrosion inhibition of mild was performed in the temperatures range of 318 to 348 K in the absence and presence of optimum concentration of inhibitor, to determine the activation energies, enthalpies and entropies of activation of the corrosion. The corresponding data are shown in Table 5.

Table 5. Various corrosion parameters for steel in 1.0 M HCl in absence and presence of optimum concentration of inhibitor at different temperatures

Temperature (K)	**Inhibitor**	C_R**(mg/cm²x h)**	η_{WL}**(%)**
318	HCl 1 M	2.1804	-
	inhibitor	0.7688	64.74
328	HCl 1 M	4.1887	-
	inhibitor	1.7567	58.06
338	HCl 1 M	7.2009	-
	inhibitor	3.6012	49.99
348	HCl 1 M	9.9982	-
	inhibitor	5.9919	40.07

Archive of SID

www.SID.ir

The comparative study of Table 5 showed that the corrosion rate increases with increase in temperature in both the inhibited solutions and uninhibited, while the efficiency of inhibiting solution decreases. A decrease in the efficiency of inhibition with increasing temperature in the presence of the studied compound may be due to the weakening of physical adsorption.

To determine the activation energy, Arrhenius equation equations 18 and 19 were use for the determination of activation energy. This provides a linear graph between ln C_R *vs* T^{-1} and is shown in Fig. 6.

$$C_R = A\, exp\left(-\frac{E_a}{RT}\right) \quad (18)$$

$$LnC_R = -\frac{E_a}{RT} + LnA \quad (19)$$

To access enthalpy of activation (ΔHa) and entropy of activation (ΔS_a), Eyring equation was used [33]:

$$C_R = \frac{RT}{Nh}\exp\left(\frac{\Delta S_a}{R}\right)\exp\left(-\frac{\Delta H_a}{RT}\right) \quad (20)$$

Where C_R is the corrosion rate, R is the gas constant, T is the absolute temperature, A the pre-exponential factor, h the Plank's constant and N is Avogrado's number, E_a the activation energy for corrosion process, ΔH_a the enthalpy of activation and ΔS_a the entropy of activation.

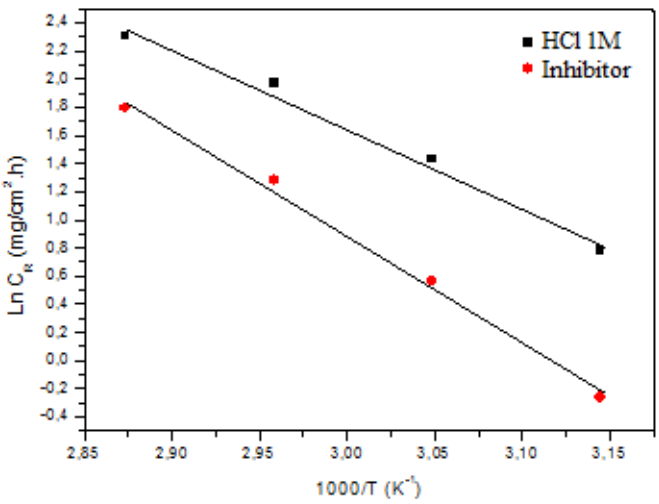

Fig. 6. Arrhenius plots of *Ln* C_R *vs*. 1/*T* for steel in 1.0 M HCl in the absence and the presence of at optimum concentration of inhibitor

Archive of SID

www.SID.ir

Figure 7 shows the variation of *Ln* (C_R/T) function ($1/T$) as a straight line with a slope of ($-\Delta H_a/R$) and the intersection of [$Ln(R/Nh)+(\Delta S_a/R)$] to determine the values of ΔH_a and ΔSa respectively. The activation parameters (E_a, ΔH_a and ΔS_a) are summarized in Table 6.

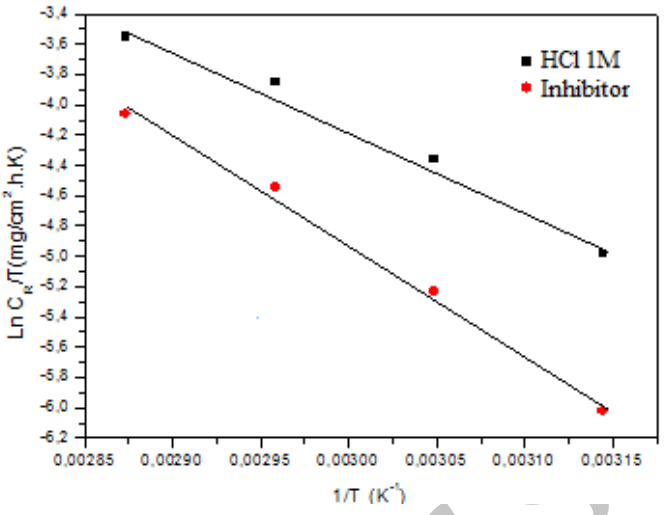

Fig. 7. Arrhenius plots of *Ln* (C_R/T) *vs.* $1/T$ for steel in 1.0 M HCl in the absence and the presence of at optimum concentration of inhibitor

It is clear from Table 6 that the value of activation energy for the inhibited solution is higher than that for the uninhibited solution, indicating that the dissolution of mild steel is decreased due to formation of a barrier by the adsorption of the inhibitor molecules on metal surface [34-36]. The variation of the activation energy (E_a) and the enthalpy of activation (ΔH_a) vary in the same way with the concentration of inhibitor, which satisfies the relationship, i.e. Ea–ΔHa=RT [37]: The positive sigh of ΔHa represents the endothermic dissolution of the mild steel.

The value of ΔS_a was lower for the uninhibited solution than that for the inhibited one. This might be attributed that the rate-determining for the activated complex follows the association pathway rather than dissociation [38].

Table 6. Activation parameters for the steel dissolution in 1.0 M HCl in the absence and the presence of inhibitor at optimum concentration

Inhibitor	E_a **(kJ/mol)**	ΔH°_a **(kJ/mol)**	ΔS°_a **(J/mol K)**	E_a-ΔH_a **(KJ/mol)**
HCl 1 M	47.19	44.42	-98.79	2.77
inhibitor	63.44	60.67	-56.4	2.77

Archive of SID

www.SID.ir

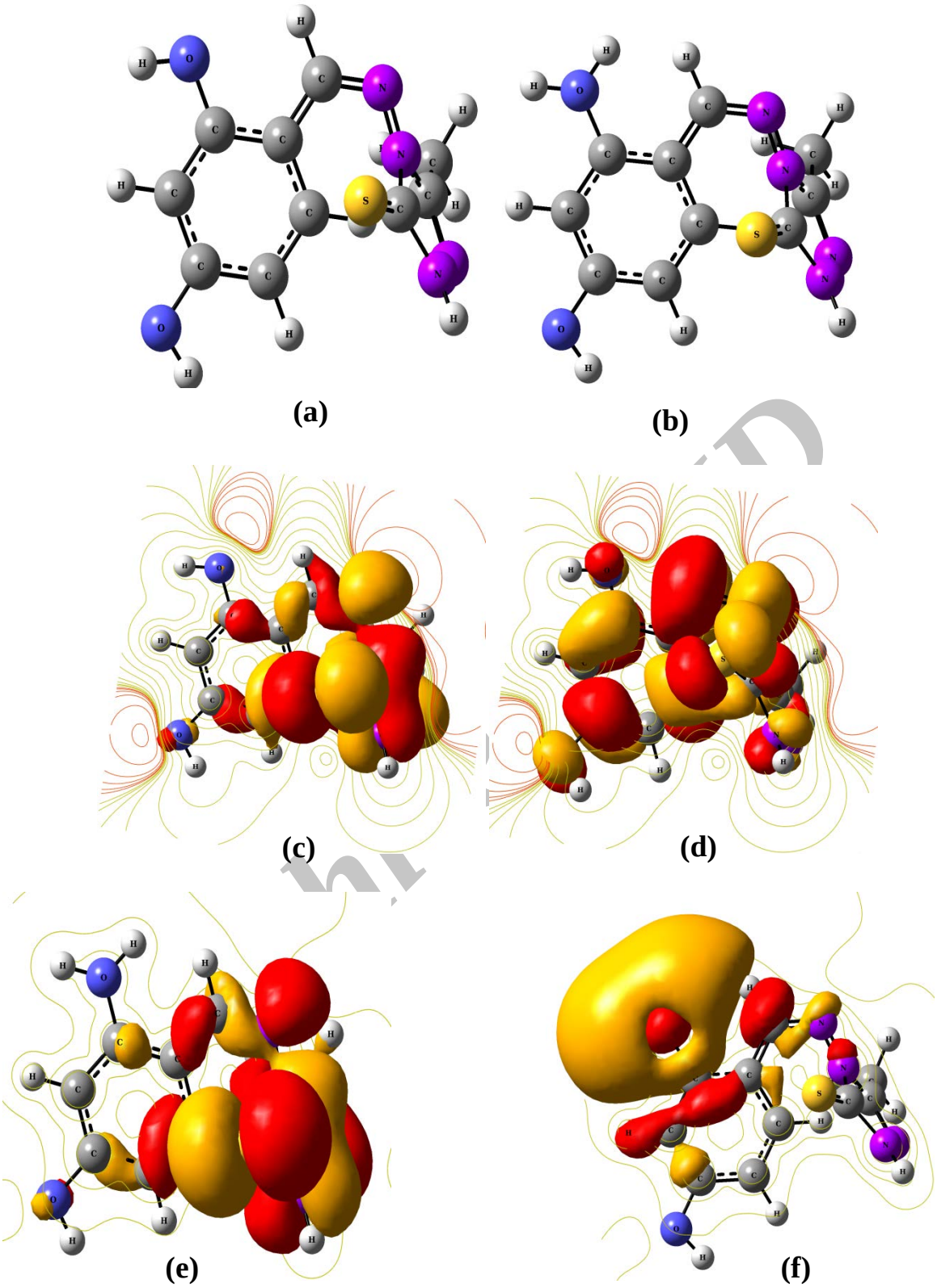

Fig. 8. The frontier molecule orbital density distributions of inhibitor: (a) optimized neutral structure (b) optimized neutral structure (c) HOMO neutral (d) LUMO neutral (e) HOMO protonated (f) LUMO protonated

www.SID.ir

3.5. Quantum chemical calculation

Quantum chemical calculations are powerful tool to understand the mechanism of inhibition and to theoretically predict the efficiency of the organic inhibitors by analyzing the global reactivity parameters, such as the E_{HOMO} of the molecule, which signifies the ability of inhibitor to donate electrons to metal, E_{LUMO} indicates the propensity of the molecule to accept electrons. The lower E_{LUMO} value reveals the greater ability of the molecule to accept electrons from metal surface. The energy gap, ΔE, is also an important parameter which indicates the reactivity of the inhibitor towards the metal surface [39]. As Δ*E* decreases, the reactivity of the molecule increases, leading to an increase in adsorption onto the metal surface. Thus, Δ*E* has been used in literature to characterize the binding ability of inhibitor molecules to the metal surface [40].

Figure 8 shows the optimized geometry, the HOMO density distribution and the LUMO density distribution of neutral and protonated inhibitor molecules.

From the figure it is observed that in the neutral and protonated forms of inhibitor, the HOMO regions are distributed over the entire triazole ring including the sulfur atom. However, in case of neutral, LUMO is distributed throughout the inhibitor molecule and in protonated it is over the –OH functional group. Therefore, before and after protonation the HOMO region almost remains intact but LUMO gets changed. Table 7 shows the calculated quantum chemical parameters.

Table 7. Calculated quantum chemical parameters of neutral and protonated inhibitor

Inhibitor	E_{HOMO}	E_{LUMO}	Δ*E*
Neutral	-5.059	-1.490	3.569
Protonated	-8.516	-5.793	2.723

As observed from Table 7 that the E_{HOMO} values of neutral form of inhibitor is higher than protonated, which supports the greater electron donation ability by neutral inhibitor as compared to protonated one. At the same time E_{LUMO} value of protonated gets lower as compared to neutral, indicating more electron acceptance from the filled metal d-orbital [41-44]. The energy gap i.e. Δ*E* is lower in protonated form of inhibitor than neutral, revealing the higher binding ability of protonated inhibitor than neutral. Thus, it is concluded on the basis of energy gap (ΔE) that protonated form triazole is better inhibitor than neutral inhibitor.

Archive of SID

www.SID.ir

3.6. Fukui index analysis

The adsorption of the inhibitor molecules on the metallic surfaces takes place by the donor-acceptor interaction, which can be analyzed by the Fukui indices. The maximum threshold values of f_k^+ and f_k^- where used to determine the nucleophilic and electrophilic behavior of different sites of the inhibitor molecules. The higher values of f_k^+ and f_k^- suggest the higher electron acceptance and electron donation respectively. The calculated Fukui indices are presented in Table 8.

Table 8. Calculated Fukui functions for the studied inhibitor molecule in aqueous phase

Atoms	f_k^-	f_k^+
C1	-0.016	0.0159
N2	0.1393	0.0073
N3	0.1513	0.0026
C4	0.0195	0.0149
N5	0.1824	-0.0039
N6	0.0967	0.1936
C7	-0.0007	0.0008
S8	0.3407	0.0498
C9	0.0139	0.2030
C10	-0.0003	0.0215
C11	0.0034	0.0448
C12	0.0006	0.0281
C13	0.0041	0.1603
C14	0.0042	0.0008
C15	0.0534	0.2325
O16	0.0002	0.0053
O17	0.0016	0.0261

Observation of table suggests that, the most susceptible sites for electrophilic attacks *i.e.*, electron donation (f_k^-) are N(2), N(3), C(4), N(5), N(6), S(8), C(9) and C(15) atoms respectively and the favorable sites for electron acceptance (f_k^+) *i.e.*, nucleophilic attacks are C(1), C(4), N(6), S(8), C(9), C(10), C(11), C(12), C(13), C(15) and O(17) respectively.

Thus, triazole and phenyl rings are actively participate in donor-acceptor interactions and which intern facilitates the adsorption of inhibitor molecule over the metal surface.

Archive of SID

www.SID.ir

4. CONCLUSSION

1. The results showed that trialzole is a very good inhibitor and showed 81% inhibition efficiency at 10^{-3} M concentration.
2. Adsorption of inhibitor at the mild steel surface in HCl solutions gave a good fit to Langmuir isotherm model. The values of Gibbs free energy of the adsorption process indicated that the adsorption of inhibitors on the mild steel surface takes place through chemical as well physical mechanism.
3. The potentiodynamic polarization curves indicated that inhibitor is a mixed type of inhibitor.
4. EIS spectra reveal that corrosion is controlled by charge transfer mechanism and inhibition occurs due to adsorption of inhibitor molecules on the metal surface.
5. The calculated quantum chemical parameters reveal that protonated form is better inhibitor than its neutral form.

REFERENCES

[1] M. A. Quraishi, and R. Sardar., Corrosion. 58 (2010) 748.

[2] S. M. Shaban, RSC Adv. 6 (2016) 39784.

[3] V. S. Sastri, Corrosion Inhibitors – Principles and Applications, Wiley, Chichester, England (1998).

[4] Y. El Ouadi, M. Elfal, A. Bouyanzer, H. Elmsellem, Y. Ramli, E.M. Essassi, N. Lahhit, A. Aouniti, A. Chetouani, and B. Hammouti. Der Pharm. Chem. 7 (2015) 354

[5] X. Lei, H. Wang, Y. Feng, J. Zhang, X. Sun, S. Lai, Z. Wang, and S. Kang, RSC Adv. 5 (2015) 99084.

[6] N. Kovacevic, and A. Kokalj, Corros. Sci. 73 (2013) 7.

[7] A. Elyoussfi, A. Dafali, H. Elmsellem, H. Steli, Y. bouzian, K. Cherrak, Y. El Ouadi, A. Zarrouk, and B. Hammouti. J. Mater. Environ. Sci. 7 (2016) 3344

[8] M. K Awad, M. R. Mustafa, and M. M. Abo Elnga, J. Mol. Struct. Theochem. 959 (2010) 66.

[9] ASTM, ASTM-G-31-72, Standard Practice for Laboratory Immersion Corrosion Testing of Metals, 1998 Annual Book of ASTM Standards, volume 03.02 – Wear and Erosion; Metal Corrosion, American Society of Testing and Materials, Philadelphia, Pennsylvania G 31–72, American Society for Testing and Materials, Philadelphia, PA, (1990).

[10] Gaussian Gaussian 03, Revision B.01, M. J. Frisch, G. W. Trucks, H. B. Schlegel, G. E. Scuseria, M. A. Robb, J. R. Cheeseman, J. A. Montgomery, Jr., T. Vreven, K. N. Kudin, J. C. Burant, J. M. Millam, S. S. Iyengar, J. Tomasi, V. Barone, B. Mennucci, M. Cossi, G. Scalmani, N. Rega, G. A. Petersson, H. Nakatsuji, M. Hada, M. Ehara, K. Toyota, R. Fukuda, J. Hasegawa, M. Ishida, T. Nakajima, Y. Honda, O. Kitao, H.

Archive of SID

www.SID.ir

Nakai, M. Klene, X. Li, J. E. Knox, H. P. Hratchian, J. B. Cross, C. Adamo, J. Jaramillo, R. Gomperts, R. E. Stratmann, O. Yazyev, A. J. Austin, R. Cammi, C. Pomelli, J. W. Ochterski, P. Y. Ayala, K. Morokuma, G. A. Voth, P. Salvador, J. J. Dannenberg, V. G. Zakrzewski, S. Dapprich, A. D. Daniels, M. C. Strain, O. Farkas, D. K. Malick, A. D. Rabuck, K. Raghavachari, J. B. Foresman, J. V. Ortiz, Q. Cui, A. G. Baboul, S. Clifford, J. Cioslowski, B. B. Stefanov, G. Liu, A. Liashenko, P. Piskorz, I. Komaromi, R. L. Martin, D. J. Fox, T. Keith, M. A. Al-Laham, C. Y. Peng, A. Nanayakkara, M. Challacombe, P. M. W. Gill, B. Johnson, W. Chen, M. W. Wong, C. Gonzalez, and J. A. Pople, Gaussian, Inc., Pittsburgh PA, 2003.

[11] W. J. Hehre, L. Radom, P. V. R. Schleyer, and A. J. Pople, Wiley-Interscience, New York (1986).

[12] J. F. Janak, Phys. Rev. B 18 (1978) 7165.

[13] R. Stowasser, and R. Hoffmann, J. Am. Chem. Soc. 121 (1999) 3414.

[14] R. G. Pearson, Inorg. Chem. 27 (1988) 734.

[15] R. G. Parr, and W. Yang, J. Am. Chem. Soc. 106 (1984) 4049.

[16] K. F. Khaled, Electrochim. Acta 55 (2010) 6523.

[17] A. S. Fouda, Y. A. Elewady, and H. K. Abd El-Aziz, J. Chem. Sci. Technol. 1 (2012) 45.

[18] X. Li, S. Deng, H. Fu, and G. Mu, Corros. Sci. 51 (2009) 620.

[19] H. Amar, A. Tounsi, A. Makayssi, A. Derja, J. Benzakour, and A. Outzourhit, Corros. Sci. 49 (2007) 2936.

[20] M. A. Deyab, S. S. Abd El-Rehim, and S. T. Keera, Colloids Surf. A 348 (2009) 170

[21] S. Haruyama, T. Tsuru, and B. Gijutsu, J. Jpn. Soc. Corros. Eng. 27 (1978) 573.

[22] L. Elkadi, B. Mernari, M. Traisnel, F. Bentiss and M. Lagrenee, Corros. Sci. 42 (2000) 703.

[23] V. Ramesh Saliyan, and A. V. Adhikari, Corros. Sci. 50 (2008) 55.

[24] A. M. Atta, O. E. El-Azabawy, H. S. Ismail, and M. A. Hegazy, Corros. Sci. 53 (2011) 1680.

[25] J.O.M., Bockris and A.K.N., Reddy, 1977. Modern Electrochemistry, vol. 2. Plenum Press, New York, p. 1267.

[26] F. Bentiss, M. Lagrenee, M. Traisnel, and J. C. Hornez, Corros. Sci. 41 (1999) 789.

[27] S. Sapra, H. Li, Z. Wang, and I. I. Suni, J. Electrochem. Soc. 152 (2005) B193.

[28] P. Agarwal, M. E. Orazem, and M. H. Garia-Rubio, J. Electrochem. Soc. 139 (1992) 1917.

[29] M. Bojinov, Electrochim. Acta 42 (1997) 3489.

[30] J. Lu, J. E. Garland, C. M. Pettit, S. V. Babu, and D. Roy, J. Electrochem. Soc. 151 (2004) G717.

[31] T. P. Zhao, and G.N. Mu, Corros. Sci. 41 (1999) 1937.

Archive of SID

www.SID.ir

[32] I. Ahamed, and M. A. Quraishi, Corros. Sci. 52 (2010) 651.
[33] Z. Szklarskasmialowska, and J. Mankowski, Corros. Sci. 18 (1978) 953.
[34] B. HAMMOUTI, A. ZARROUK, S.S. AL-DEYAB and I. WARAD, Oriental Journal of Chemistry, 24 (2011) 23.
[35] F. Bentiss, M. Lebrini, and M. Lagrenée, Corros. Sci. 47 (2005) 2915.
[36] I. Dehri, and M. Özcan. Mater. Chem. Phys. 98 (2006) 316.
[37] G. K. Gomma, and M. H. Wahdan, Mater. Chem. Phys. 39 (1995) 209.
[38] N. M. Guan, L. Xueming, and L. Fei, Mater. Chem. Phys. 86 (2004) 59.
[39] X. Li, S. Deng, H. Fu, and G. Mu, Corros. Sci. 50 (2008) 2635.
[40] K. R. Ansari, M. A. Quraishi, and A. Singh, Corros. Sci. 79 (2014) 5.
[41] A. Aytac, S. Bilgic, G. Gece, N. Ancin, and S.G. Oztas, Mater. Corros. 63 (2012) 729.
[42] M. A. Amin, K. F. Khaled, and S. A. Fadl-Allah, Corros. Sci. 52 (2010) 140.
[43] G. Gece, and S. Bilgic, Corros. Sci. 51 (2009) 1876.
[44] E. E. Ebenso, D. A. Isabirye, and N. O. Eddy, Int. J. Mol. Sci. 11 (2010) 2473.
[45] I. A. hamad, S. Khan, K. R. Ansari, M. A. Quraishi, Primaquine: J. Chem. Pharm. Res. 3 (2011) 70.

Archive of SID

Copyright © 2017 by CEE (Center of Excellence in Electrochemistry)
ANALYTICAL & BIOANALYTICAL ELECTROCHEMISTRY (http://www.abechem.com**)**
Reproduction is permitted for noncommercial purposes.

www.SID.ir